Incorporated diffusion ordered heteronuclear multiple bond correlation spectroscopy, 3D iDOSY-HMBC. Merging of diffusion delay with long polarization transfer delay of HMBC

Jesus Perea-Buceta, Daniel Rico del Cerro, Ilkka Kilpeläinen, Sami Heikkinen *

Department of Chemistry, University of Helsinki, P.O. Box 55, FIN-00014 Helsinki, Finland

ARTICLE INFO

ABSTRACT

3D iDOSY-HMBC pulse sequences allow the simplification of HMBC data of mixtures via separation in the diffusion domain. The presented methods utilize incorporated DOSY approach, iDOSY, where the existing delays of the basic pulse sequence are utilized for diffusion attenuation. In the simplest form of the proposed 3D iDOSY-HMBC sequences, no extra delays or RF-pulses were required, only two diffusion gradients were added within HMBC polarization transfer delay.

© 2020 The Authors. Published by Elsevier Inc. This is an open access article under the CC BY license (http://creativecommons.org/licenses/by/4.0/).

1. Introduction

Diffusion ordered spectroscopy, DOSY as well as diffusion weighted NMR experiments have established their place in modern NMR methods [1–8]. Numerous diffusion-based experiments started to emerge in 1990′s and ever since diffusion weighted/DOSY versions of common homonuclear as well as heteronuclear experiments have been developed, like COSY [9], NOESY [10], TOCSY [11], J-resolved [12], INEPT [13], HMQC [14], HSQC [15], TROSY [16]. Up to date, practically all the pulse sequences routinely utilized in organic chemistry-oriented NMR have been modified into corresponding diffusion versions.

While in diffusion weighted experiments the original dimensionality of the experiment is preserved, in DOSY versions an additional diffusion encoding is applied to create an additional diffusion dimension, where the correlation peaks appear at characteristic diffusion coefficient values. The diffusion coefficients (D) are classically calculated by fitting the Stejskal-Tanner equation [6,7,17,18] to the attenuating intensities in the series of 1D or 2D spectra recorded with increasing diffusion gradient strengths (Eq. (1)).

$$I_{g_D} = I_0 e^{\left(-D\gamma^2\delta_D^2\sigma^2 g_D^2\Delta'\right)} \tag{1}$$

In Eq. (1) I_{gD} and I_0 are the signal intensities in presence and in absence of the diffusion gradient, respectively, D is the diffusion coefficient, γ is the gyromagnetic ratio of the nucleus in question (or depending on the coherence transfer pathway, a linear combination of gyromagnetic ratios of the studied nuclei), δ_D is the diffusion gradient duration, σ is the shape factor for the diffusion gradient, g_D is the diffusion gradient strength and Δ' is the corrected diffusion delay. The value for Δ' depends on the timings and setup of the applied pulse sequence as well as on the shape of the diffusion gradient pulse utilized. For quantitative diffusion coefficient studies, it is important to apply precise Δ' values for the best accuracy as described by Sinnaeve.[18] The resulting cross peak shape in the diffusion dimension is represented by a Gaussian peak shape with the intensity and position obtained from the fit and the line width from the standard deviation or standard error of the fit [1].

DOSY is a powerful method to study mixtures by resolving the spectra of the individual components based on their diffusion rate, allowing a direct simplification of the NMR data of a mixture, thus alleviating the qualitative analysis. Separation in the diffusion dimension can be enhanced by utilizing suitable additives in the NMR sample to modify the diffusion rate of the mixture components via interaction with the added compounds (matrix assisted DOSY or NMR chromatography) [19–28]. DOSY has also been successfully utilized in studying intermolecular interactions, supramolecular chemistry and molecular size estimation [29–31].

---

* Corresponding author.
  E-mail address: Sami.Heikkinen@helsinki.fi (S. Heikkinen).

Also, the implementation of a diffusion weighting propagator in a 1D or 2D method is a viable approach to suppress signals from rapidly diffusing species, provided that the compound of interest has a markedly slower diffusion rate [32]. This approach can be readily used in non-deuterated multi-solvent or, more recently, in ionic liquid systems containing several intense signals hampering the analysis [33,34].

In order to incorporate a diffusion domain, or diffusion weighting capabilities, into an existing NMR pulse sequence, it is possible to utilize classic spin-echo element with two gradient pulses (diffusion gradients) separated by a delay (diffusion delay) during which the signal attenuation due to diffusion takes place. An even simpler approach would be just to attach two diffusion gradient pulses of opposite polarity separated by a delay $i.e.$ to form a gradient echo. Diffusion propagators are normally designed to affect ^1H magnetization due to high gyromagnetic ratio of ^1H and thus high response to magnetic field gradients. Therefore, in the following we limit the discussion to ^1H magnetization during diffusion periods. In the aforementioned setups, spin echo and gradient echo, ^1H magnetization is transverse throughout the whole diffusion delay. In the spin-echo setup, the effects of chemical shift evolution as well as possible heteronuclear coupling evolution are eliminated by the applied 180° ^1H-pulse in the center of the spin-echo delay. Homonuclear ^1H–^1H coupling constants (J_{HH}), are still evolving during the lengthy diffusion delay generating distortions into multiplet line shapes (J-modulation). In the gradient echo setup, the evolution of chemical shifts as well as homo- and heteronuclear couplings during the diffusion delay will lead to even larger distortions. In both spin-echo and gradient echo methods, the signals will be also attenuated by T_2-relaxation and this could be significant for larger molecules with $T_2 \ll T_1$. Currently, Bipolar Pulse Pair STimulated Echo (BPPSTE) [7,8] is probably the most frequently utilized pulse sequence for 2D ^1H DOSY and is also incorporated into a wide array of other sequences to introduce diffusion weighting/DOSY. The benefits of BPPSTE are the suppression of eddy current effects on the line shape as well as the fact, that relevant magnetization is along the ±z-axis during the relatively long diffusion delay, typically around 50–500 ms, and thus subject to T_1-relaxation rather than T_2. Furthermore, the effects from J-modulation are small, provided that the time the magnetization spends in the transverse plane can be kept short $i.e.$ the durations of the four diffusion gradients. The selection of longitudinal magnetization during the diffusion delay further suppresses the effects of J-modulation in the multiplet line shapes. It should be noted, however, that only half of the magnetization can be preserved in BPPSTE as a result of selecting exclusively longitudinal components during the diffusion delay.

As stated before, diffusion weighting only requires dephasing and rephasing gradients and a certain delay in between. Therefore, the pulse sequences using field gradient pulses for coherence selection are practically always, at least to some degree, diffusion weighted. Thus, if the original pulse sequence contains a sufficiently long propagator of fixed duration, like mixing in NOESY [35] or TOCSY [35] or constant time t_1-evolution in CT-HSQC [36,37], or any constant time experiment, then instead of adding an extra BPPSTE, the existing period can be readily utilized for diffusion weighting/DOSY and the level of diffusion weighting can be controlled by the durations and strengths of coherence selection gradient pulses. Merging of diffusion weighting into 2D NMR pulse sequences to acquire 3D ^1H DOSY datasets was originally introduced by Birlirakis and Guittet for TOCSY, NOESY and ROESY as well as for double quantum correlation experiment [35]. This merging concept is currently known as iDOSY, indicating that the diffusion time and diffusion gradients are incorporated into the main pulse sequence, like in mixing time in iDOSY-NOESY, and

no separate diffusion element is required. Several iDOSY modifications of typical pulse sequences have emerged by now [36–41] and some of the recent modifications provide remedies to the important problem of spectral overlap complicating the DOSY-analysis [42,43]. The time available for diffusion editing in the iDOSY-approach is not freely selectable and depends on the original sequence. Therefore, the application of this methodology will have limitations in separation of mixtures of slowly diffusing molecules [11], but would be useful with the small and medium sized compounds, which are typically encountered in organic chemistry-oriented NMR. Furthermore, in case of mixtures consisting of macromolecule and small molecules in non-viscous solutions, the limited diffusion time available in the iDOSY approach is frequently sufficient for suppressing signals of small molecules. In favorable cases, even complete diffusion filtration of small molecule signals could be possible with acceptable signal losses for the large molecule of interest. Obviously, this normally requires major differences in diffusion coefficients. The iDOSY approach can be directly utilized in HMBC experiments [44–47], as these inevitably contain a lengthy polarization transfer delay required for the evolution of small heteronuclear long-range couplings. For ^1H–^{13}C-systems, long range coupling constant values $^nJ_{CH}$ (n = 2–4) can range from −10 to 20 Hz, excluding the extreme values in acetylenes. The typical $^{2-3}J_{CH}$ values range from ±2 to ± 10 Hz. For setting up ^1H–^{13}C HMBC, classically one $^nJ_{CH}$ value is selected (typically 5–10 Hz), to calculate the polarization transfer delay. Frequently selected $^nJ_{CH}$-value of 7 Hz for setting up the polarization transfer delay translates into 71.4 ms delay (1/2^n-J_{CH}) which, from the DOSY/diffusion weighting point-of-view, is often sufficient to obtain decent suppression of signals of small molecules or to achieve proper separation in the diffusion domain of DOSY-type data for different sized molecules. Furthermore, there is no need to consider line shape distortions due to J_{HH} or chemical shift evolution during the diffusion delay, since these evolutions will inevitably be present in normal HMBC as well and since the HMBC data is processed in magnitude mode. Previously, Stchedroff $et\ al.$ [38] have successfully utilized the idea of using long delays within the long-range coupling constant optimized HMQC-iDOSY for ^1H–^{29}Si-systems, where both long polarization transfer delay and the refocusing delay were used for diffusion labeling. However, to the best of our knowledge, the iDOSY-approach has not been implemented to a classic HMBC experiment in order to create 3D DOSY-HMBC data. Instead, the existing 3D DOSY-HMBC sequences have directly incorporated an extra diffusion propagator, like BPPSTE-LED (LED; Longitudinal Eddy-current Delay), into the HMBC sequence [7,8,48]. DOSY-HMBC is an important complementary experiment to the existing hyphenated DOSY-variants of HSQC, COSY, NOESY or TOCSY, providing essential structural characterization data for intact mixtures. The lower sensitivity of HMBC and the fact, that a successful DOSY processing requires decent signal-to-noise ratio, normally translates into required higher sample concentrations and/or prolonged accumulation times. In the current study, the concept of merging the diffusion period with polarization transfer delay of ^1H–^{13}C HMBC enables the design of 3D incorporated diffusion ordered HMBC pulse sequences, 3D iDOSY-HMBC, eliminating the need for extra diffusion propagator (BPPSTE-LED in DOSY-HMBC) [7,8,48] and thus significantly shortening and simplifying the sequence. In the 3D iDOSY-HMBC setup, the loss of half of the signal due to BPPSTE is avoided. This, and also the obtained general reduction in the pulse sequence duration as well as the reduction in the number of RF-pulses, will have a positive impact on the sensitivity. In the simplest form, addition of just two gradient pulses in a normal HMBC pulse sequence is sufficient without any need for extra delays or RF-pulses.

2. Results and discussion

The 3D iDOSY-HMBC pulse sequences used in this study are presented in Fig. 1. The version **A** is a normal magnitude mode, gradient selected HMBC with a simple gradient-enhanced first-order low-pass filter [46,47,49] incorporating gradient echo type (opposite polarities) diffusion encoding/decoding gradient pulses (duration δ_D, strength g_D) separated by diffusion delay (Δ_D) within the polarization transfer delay (Δ_{LR}). Compared to normal HMBC, the only difference is the additional two diffusion gradients. The available diffusion time Δ_D for pulse sequence **A** depends on polarization transfer delay Δ_{LR}, duration of the low-pass filter gradient g_1, duration of the diffusion gradient δ_D and eddy current recovery delays τ_e. The encoding diffusion gradient is applied after the low-pass filter gradient g_1 and the decoding diffusion gradient g_D is applied just before the 90° ^{13}C-pulse preceding the t_1-period (ϕ_5). The relation for diffusion delay Δ_D is shown in Eq. (2).

$$\Delta_D = \Delta_{LR} - g_1 - \delta_D - 2\tau_e \tag{2}$$

This setup allows relatively free selection of diffusion gradient duration, which would not be the case if the first diffusion gradient was positioned within the low-pass filter period (τ). Obviously, the hardware safety limits regarding the gradient amplitude and duration will cause some restrictions. From the point of eddy currents, there are no similar self-compensation, that could be obtained by utilizing BPPSTE-type [9] diffusion gradients. However, with modern NMR probes incorporating actively shielded gradients and with shaped gradient pulses followed by recovery delays of 100–500 µs, the induced eddy current effects remain small. These effects are predominantly reflected as signal phase distortions [6], which are efficiently masked for the pulse sequences shown in Fig. 1, as magnitude mode presentation is utilized for the resulting spectra. A point worth mentioning is, that for improved suppression of direct HMQC-type correlations, one can apply also higher order low-pass filters [50] of different types instead of a simple first order low-pass filter utilized in pulse sequence **A**.

Higher order low-pass filters further extend the total duration of the HMBC sequence. If such filter would be incorporated in sequence **A** to replace the 1st order low-pass filter, then the added duration would not be used for diffusion purposes. Instead, the pulse sequence **B** in Fig. 1 offers a natural possibility to slightly prolong (approximately 15 ms) the available diffusion time via the duration of 3rd order low-pass filter [50]. Also, in this approach, the number of RF-pulses and the total duration of the sequence remain the same compared to the original HMBC with 3rd order low-pass filter, the only difference being the two diffusion gradients (g_D), the one applied immediately after the first 90° ^{1}H-pulse and the second just before the fourth 90° ^{13}C-pulse. Obviously, the obtainable addition to diffusion time is only moderate, and could be meaningful mainly for relatively small molecules, especially if the experiment is aiming to suppress solvent signals *i.e.* diffusion edited 2D HMBC. It should be also noted that in the presented setup of pulse sequence **B**, the diffusion gradient pulse duration δ_D is now limited by the durations of the first low-pass filter element (τ_1) and the embedded low-pass filter gradient (g_1). Naturally, this limitation could be overcome by the addition of an extra 180° pulse on either channel and a delay. The total diffusion delay for pulse sequence **B**, neglecting the durations of the three low-pass filter 90° ^{13}C-pulses, is shown in Eq. (3).

$$\Delta_D = \tau_1 + \tau_2 + \tau_3 + \Delta_{LR} - \delta_D - \tau_e \tag{3}$$

For longer diffusion times beyond the available polarization transfer delay, a simple modification is shown in pulse sequence **C**, where an extra delay period is added to extend the diffusion time. In order to refocus ^{n}J$_{CH}$-evolution during this delay, a 500 µs wideband adiabatic ^{13}C inversion pulse (AS) is applied in

the center, leaving ^{1}H-magnetization untouched and thus the applied pulse does not interfere with diffusion encoding as it would be the case if 180° ^{1}H-pulse were applied instead (need to invert diffusion gradient polarity, effects on diffusion decoding due to imperfect inversion). In pulse sequence **C**, the total duration of additional delay is $2\delta_1 + AS$. The required δ_1-delay duration (Eq. (4)) depends on the desired diffusion time Δ_D, polarization transfer delay Δ_{LR}, the width of adiabatic ^{13}C-inversion pulse AS, gradient g_1 duration, diffusion gradient duration δ_D and eddy current recovery delays τ_e.

$$\delta_1 = (\Delta_D - \Delta_{LR} + g_1 + \delta_D + 2\tau_e - AS)/2 \tag{4}$$

The decoding diffusion gradient is applied in the end of the second δ_1-delay, just before the 90° ^{13}C pulse (ϕ_5) preceding the t_1-period. If extensive diffusion times are needed *i.e.* hundreds of milliseconds, it is probably better to rely on BPPSTE-type modifications [7,48], as their relaxation conditions during the diffusion time are more favorable (longitudinal magnetization, T_1-relaxation). For moderate diffusion time extension requirements pulse sequence **C** could be useful, though.

The aforementioned pulse sequences can be readily converted into versions utilizing bipolar diffusion gradients. An example is displayed in the pulse sequence **D** (Fig. 1) which presents a modification of the pulse sequence **B**. Like pulse sequence **B**, the pulse sequence **D** also incorporates 3rd order low-pass filter to prolong the available diffusion time. In sequence **D**, however, bipolar gradient pulses are used for diffusion encoding/decoding. In addition, the diffusion encoding period just after the first 90° ^{1}H-pulse is completely an additional propagator separate from the low-pass filter and thus allows free adjustment of the diffusion gradient duration, obviously within the hardware limitations. Naturally, this adds to the total duration of the pulse sequence. The second diffusion gradient pair is applied in the end of the polarization transfer delay. In order to allow ^{n}J$_{CH}$ to evolve during this final diffusion gradient period, 180° pulses must be applied on both ^{1}H- and ^{13}C-channels. In the pulse sequence **D**, a 500 µs wideband adiabatic inversion pulse (AS) on ^{13}C-channel was used. In order to keep timings similar in both diffusion labeling periods *i.e.* to keep bipolar diffusion gradient temporal distance the same, a delay (δ_2) was added to flank 180° ^{1}H-pulse in the initial diffusion encoding element. This is not actually necessary, as these experiments are not aiming for quantitative diffusion coefficient measurements, but instead utilize different diffusion properties to simplify the HMBC spectra of mixtures. The available diffusion delay Δ_D in sequence **D** depends on the delays needed for 3rd order low-pass filter, τ_{1-3}, and the polarization transfer delay, Δ_{LR} (Eq. (5)). As for Eq. (3), the durations of ^{13}C-pulses in low-pass filter are neglected.

$$\Delta_D = \tau_1 + \tau_2 + \tau_3 + \Delta_{LR} \tag{5}$$

The benefits of sequence **D** are the freedom of selecting the diffusion gradient duration, utilization of the 3rd order low-pass filter duration in the diffusion time, and the minimized effects of eddy currents due to the self-compensating nature of bipolar diffusion gradient pulses as well as reduced effects on the deuterium lock signal. The required extra 180° pulses can be considered as a minor drawback, since an additional phase cycling or gradient techniques would be needed to eliminate the effects of imperfect pulses, which mostly lead to errors in the obtained diffusion coefficients. However, with the good RF-homogeneity of modern instruments, the effects of imperfect 180° pulses can be reduced sufficiently enough without need to expand the phase cycle or do other corrective measures. Especially, for the accumulation of 3D data, the expansion of phase cycle would easily double/quadruple the required measurement time.

All the proposed pulse sequences here are designed for simplifying the HMBC data of mixtures through diffusion dimension (3D)
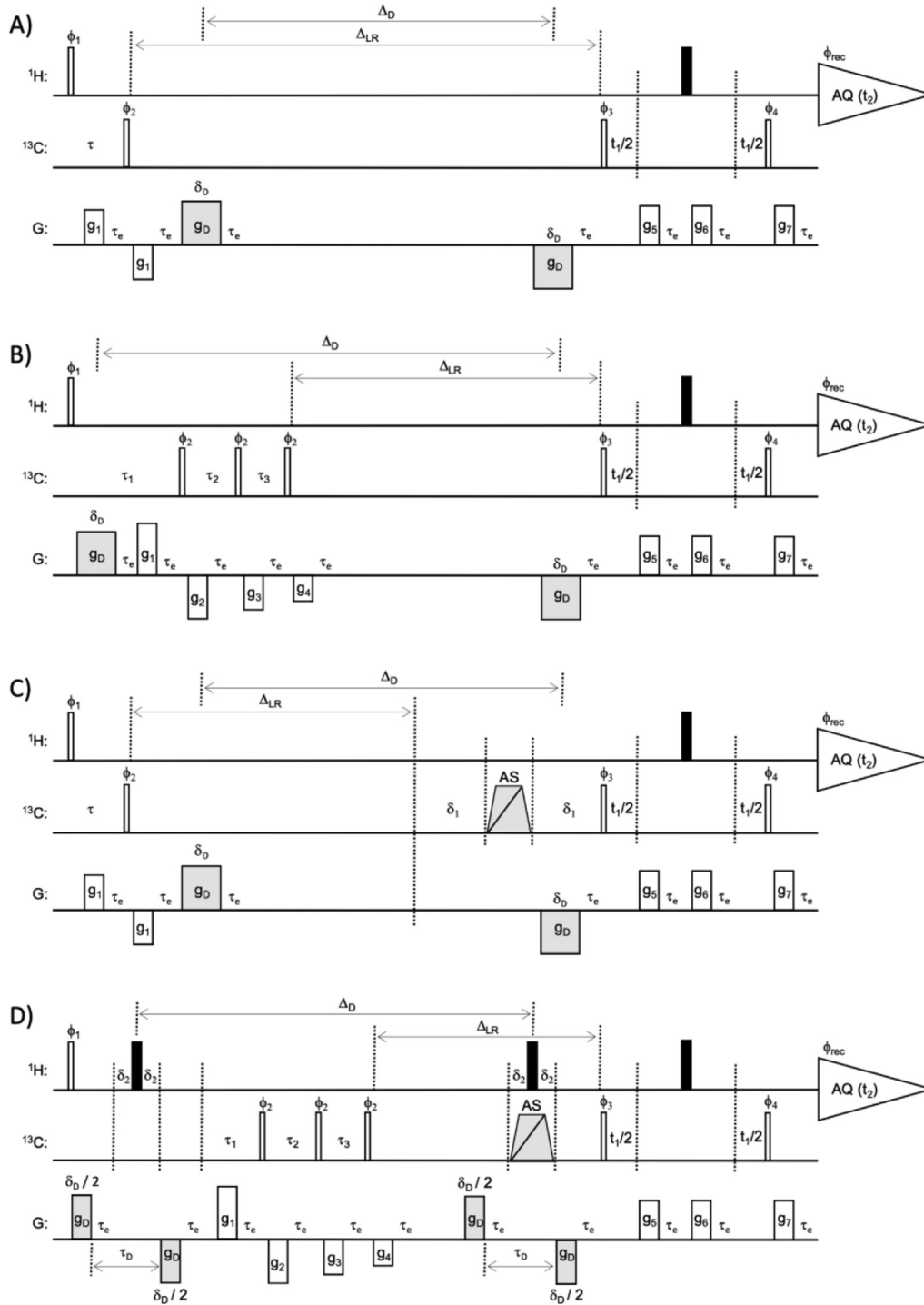
Fig. 1. The 3D iDOSY-HMBC pulse sequences. a) Pulse sequence **A** with 1st order low-pass filter and utilizing gradient echo type diffusion gradients within polarization transfer delay; b) Pulse sequence **B** with 3rd order low-pass filter and gradient echo type diffusion gradients. Low-pass filter incorporated in the diffusion delay; c) Pulse sequence **C** with 1st order low-pass filter and utilizing gradient echo type diffusion gradients. Extra delay period after polarization transfer delay to prolong diffusion time; d) Pulse sequence **D** with 3rd order low-pass filter and bipolar diffusion gradients. Narrow white rectangles correspond to 90° hard rectangular pulses, while wide black/white rectangles represent 180° pulses. Carbon pulses denoted by *AS* and marked by gray trapezoid represent adiabatic, frequency-swept wideband inversion smoothed CHIRP pulses [51]. The delay Δ_D represents the diffusion time while Δ_{LR} is the polarization transfer delay for heteronuclear long-range couplings, $1/(2^nJ_{CH})$. The delay duration for 1st order low-pass filter is $\tau = 1/(2^1J_{CHave})$, whereas for 3rd order filter the durations are $\tau_1 = 1/(2^1J_{CHmin} + 0.14(^1J_{CHmax}-^1J_{CHmin}))$, $\tau_2 = 1/(^1J_{CHmin}+^1J_{CHmax})$ and $\tau_3 = 1/(2^1J_{CHmax} - 0.14(^1J_{CHmax}-^1J_{CHmin}))$ [50], where $^1J_{CHave}$, $^1J_{CHmin}$ and $^1J_{CHmax}$ represent estimated average, lowest and highest values for $^1J_{CH}$ coupling in the studied system, respectively. Delay δ_1 in sequence C is used to independently extend diffusion delay Δ_D beyond Δ_{LR}, whereas delay δ_2 considers duration difference between hard rectangular 180° ^1H-pulse and adiabatic ^{13}C-pulse *AS* and is applied to keep the timings of both bipolar gradient pairs similar. The symbol τ_D in pulse sequence **D** indicates the total delay in between the bipolar gradient pulse pair. Gray rectangles denoted by g_D represent diffusion gradients (Z-axis) with duration of δ_D ($\delta_D/2$ for bipolar gradient pulse setup of sequence **D**) while other gradient pulses are presented by white rectangles with g_1–g_6 denotation. Gradient pulses g_1–g_4 are used for low-pass filtering (Y-axis) while the gradients g_5 and g_6 and g_7 are for coherence selection (XZ-axis). Each gradient pulse is followed by an eddy current recovery delay, τ_e. The phase of all RF-pulses is ×, unless otherwise indicated. The phase cycles for the pulse sequences: ϕ_1 = x, −x, ϕ_2 = 4(x), 4(-x), ϕ_3 = 2(x), 2(-x), ϕ_4 = 8(x), 8(-x), ϕ_{rec} = x, 2(-x), x, x, 2(-x), x, -x, 2(x), -x, -x, 2(x), -x. The spectra were acquired in magnitude mode. Axial peak displacement was obtained via the States-TPPI method by inverting phase ϕ_3 and receiver ϕ_{rec} on every second increment [52].

/ diffusion filtration of small molecule signals (2D) and not to provide quantitative diffusion coefficient data. In the presented sequences, several field gradient pulses are utilized (diffusion gradients, low-pass filter gradients, coherence selection gradients). Since a set of 2D spectra with varying diffusion gradient amplitudes are recorded to create the final 3D data, there is a possibility for inadvertent refocusing of unwanted magnetization via interaction with other gradient pulses. To minimize the aforementioned risk, a careful planning of gradient amplitudes and/or durations is in place if all gradients are applied along same physical axis (typically Z-axis). Also, any additional gradients applied to non-zero coherences in-between the diffusion encoding/decoding gradients using the same gradient axis, will have an impact on the diffusional signal attenuation. These extra gradients, as well as the diffusion gradient shapes, have an effect on the delay Δ' of Eq. (1) and for quantitative and precise diffusion coefficient values, these have to be taken into account in the diffusion domain processing [18]. The aforementioned conditions, excluding the gradient shape effects, can be alleviated via triple axis gradient system. When using gradient axis orthogonal to the diffusion gradients for any additional gradients during the diffusion delay (pulse sequences **B** and **D**), the interference of the intervening gradients on the resulting calculated diffusion coefficients can be ignored [18]. Also, the application of orthogonal gradient axis on coherence selection gradients avoids artefacts arising from accidental recalling of unwanted magnetization. Therefore, all the pulse sequences presented in Fig. 1 have been tested utilizing Z-gradients for diffusion attenuation, Y-gradients for low-pass filters and XZ-gradients for coherence selection. Other important factors affecting the calculated diffusion coefficients are the noise (including t_1-noise, which can be substantial for the most intense signals) and convection. The noise adds to all 2D peak volumes in magnitude mode experiments and this will result in some underestimation in the calculated diffusion coefficients. If required, this could be suppressed via baseline correction and/or t_1-noise reduction procedures. Convection within the sample affects the diffusion measurements and is very prevalent with low-viscosity samples and/or with elevated temperatures. In cases, where the convection is very fast, the proposed pulse sequences as such cannot be directly utilized. In these situations, some means to attenuate the convection effects must be applied, for instance performing the measurements in ambient temperature without temperature control and gas flow, reducing sample height or changing solvent to a more viscous one, to mention some [53,54]. Alternatively, convection compensation could be applied in the presented pulse sequences by modifying the diffusion gradient setup. As the diffusion period here is based on gradient echo, the convection compensation could be arranged without sensitivity penalty [38,53,54]. In presence of slow convection with the proposed, uncompensated pulse sequences, the obtained diffusion coefficients will be obviously affected (increased apparent diffusion coefficients), but still allowing separation in the diffusion domain. However, as stated above, the purpose of these iDOSY-HMBC sequences is solely to provide qualitative information for mixtures via simplification of HMBC data using the extra separation obtained from diffusion domain, and thus the requirements regarding the diffusion coefficient precision are lower. The pulse sequence code in Bruker format for experiments **A-D** is available in the Supplementary Material.

Fig. 2 shows the 3D iDOSY-HMBC spectrum of the test mixture recorded using the sequence **A** and the 2D-projection along ^{13}C-axis (effectively resembling traditional 2D ^{1}H-DOSY) is included to further illustrate the component separation in diffusion domain. Also, the structural formula and numbering for compounds of the test mixture, brucine (0.15 M), *n*-propanol (3.34 M), methanol (6.14 M) and toluene (2.35 M) are shown. The ^{1}H and ^{13}C NMR-assignments for the test mixture are given in the Supplementary

Material. The positions along diffusion axis (logD) for the individual components are marked in both spectra. While the four components of the test mixture are separated in the diffusion domain, as can be seen in the 2D ^{1}H DOSY projection, some overlap due to the width of the diffusion peaks in the corresponding domain exists. This would lead to leaking of the residual peaks into the spectrum of another component with diffusion coefficients close by.

Figs. 3 and 4 display the 2D HMBC slices taken from the logD-locations illustrated in Fig. 2. The HMBC slices are shown for pulse sequences **A** and **B**. The 2D HMBC slices shown in Fig. 3 correspond faster diffusing species in the test mixture, toluene, -8.77 log(m^2/s), methanol, -8.84 log(m^2/s) and *n*-propanol -8.92 log(m^2/s). Even though the diffusion coefficients (logD) for these are quite similar and the "tails" of the peaks in the diffusion domain can extend into reach another component's logD-plane, relatively clean HMBC spectra can be obtained with proper threshold settings. Obviously, leaking of one component's spectrum into another is more difficult to avoid if there is a significant difference in the signal intensities between the two components. For example, in the HMBC slices for methanol (Fig. 3B and E), there are no actual HMBC correlations and the only methanol originated signal would be a small residual direct ^{1}H–^{13}C correlation due to imperfect low-pass filtration (marked by red arrows in Fig. 3B). The corresponding signals are not visible in Fig. 3E, that shows the HMBC slice recorded with sequence **B** utilizing 3rd order low-pass filter and plotted using the same threshold as Fig. 3B. Both spectra contain spurious signals (marked by red asterisks) originating from large HMBC correlations belonging to protons of the methyl group in toluene (T7, 2.28 ppm) as well as *n*-propanol methylene (P2, 1.56 ppm) and methyl (P3, 0.93 ppm). The "tails" of these peaks extending into logD-plane of methanol in the diffusion domain are small, but of comparable intensity to the aforementioned residual direct ^{1}H–^{13}C correlation of methanol and thus appear in the spectra. In case of toluene and *n*-propanol, clean HMBC spectra of the components can be obtained. The prominent differences between the spectra recorded with sequence **A** and **B** are the residual ^{1}H–^{13}C direct correlations visible in Fig. 3A-3C (red arrows), as a result of 1st order vs. 3rd order low-pass filter performance.

Fig. 4 presents the brucine slices, -9.27 log(m^2/s), from 3D iDOSY-HMBC data recorded using sequences **A** (Fig. 4A) and **B** (Fig. 4B) as well as the classic gradient selected HMBC with 1st order low-pass filter (Fig. 4C). Red rectangles in the reference HMBC spectrum (Fig. 4C) indicate the signals originating from toluene, methanol and *n*-propanol. These signals of high concentration components are well below the threshold in the iDOSY-HMBC-slices shown in Fig. 4A and 4B indicating that the 3D iDOSY-HMBC allows retrieval of a clean HMBC spectrum for brucine. Obviously, some minor signals from other mixture components can still be seen at the presented threshold, marked by red asterisks. Generally, spurious signals originating from other mixture components in the HMBC spectra of brucine are small, given the large concentration differences between the test mixture components (0.15 M brucine, 3.34 M *n*-propanol, 6.14 M methanol, 2.35 M toluene). This can be readily observed in Fig. 5, where 1D ^{1}H-projections are taken from HMBC slices of the individual components of the test mixture (Fig. 3A-3C, 4A). The spurious signals are marked by red asterisks in the spectra. Also, the assignments for faster diffusing components methanol, *n*-propanol and toluene are provided in the corresponding projections. Generally, all spurious signals contaminating the spectrum of the actual component remain at low level except for the methanol projection, where the actual signal is already small (resulting from imperfect low-pass filtration). In the brucine projection, the smallest brucine signal belonging to proton B22 at 5.8 ppm is closest to spurious signals in intensity, but remains larger. The performance of presented method suggest, that it can be useful in separating the
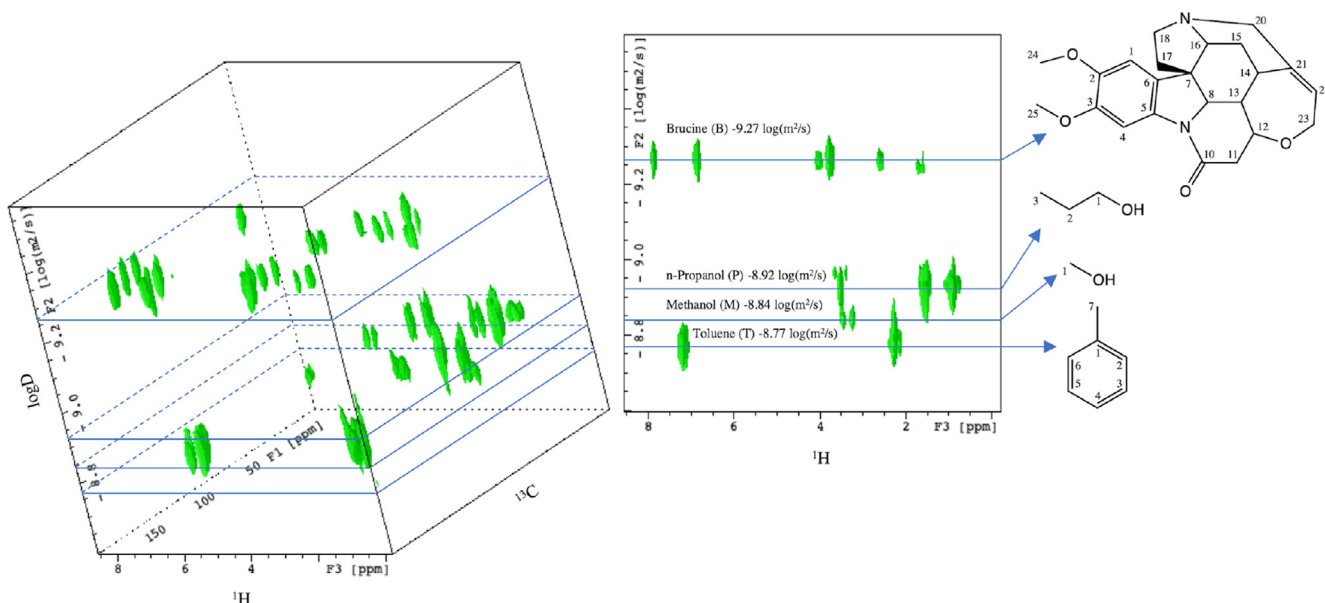
Fig. 2. 3D iDOSY-HMBC spectrum of the test mixture recorded using the sequence **A** (left) and 2D ^{1}H DOSY projection along ^{13}C-axis of the same data (right) as well as structural formulas and numbering for molecules in the test mixture; brucine (B), *n*-propanol (P), methanol (M), and toluene (T). The 2D HMBC plane positions along the logarithmic diffusion axis (logD) for the individual components are marked in both 3D spectrum and 2D projection.

HMBC spectrum of larger target component from smaller molecular size high concentration solvent signals and also impurities, the situations that are frequently encountered in synthetic organic chemistry.

Fig. 6 presents 2D ^{1}H DOSY projections of 3D iDOSY-HMBC spectra recorded using pulse sequences shown in Fig. 1. In addition, a normal 2D ^{1}H DOSY recorded using the BPPSTE-LED pulse sequence [7,8] is presented for comparison. The projections were obtained by taking the sum of all 2D planes along the ^{13}C-axis, effectively resulting in a data, that is comparable to 2D ^{1}H DOSY. The individual vertical scaling for each projection as well as for reference BPPSTE-LED data was utilized. The projection spectra were scaled according to DOSY correlation of brucine B22 at 5.82 ppm. As can be observed in Fig. 6, all the suggested pulse sequences produce essentially similar data, that agrees with the reference BPPSTE-LED experiment. The separation and resolution in the diffusion dimension is similar for each method, and the sequences **C** and **D** will perform equally as shown for sequences **A** and **B** in Figs. 3 and 4. The DOSY-correlation marked by a red rectangle in Fig. 6E belongs to exchanging protons of residual water and the hydroxyl proton of methanol (hydroxyl proton signal of *n*-propanol at 5.25 ppm is below the threshold). This marked peak is missing from 2D ^{1}H DOSY projections in Fig. 6A–D, obviously since there are no existing HMBC-correlations for the related protons. The times, that magnetization spends on transverse plane prior to t_1-period (diffusion times Δ_D in parentheses) are 74.9 ms (67.5 ms), 81.9 ms (81.5 ms), 87.3 ms (80.0 ms) and 85.3 ms (83.2 ms) for iDOSY-HMBC pulse sequences **A-D**, respectively. These differences will naturally also cause variation in sensitivities and thus the comparison will be semi-quantitative, at best. All sequences are capable of providing data of comparable quality, although some minor sensitivity differences are present. As the 2D projection spectra (Fig. 6A–D) are approximately scaled according to DOSY peak at 5.82 ppm, qualitative comparison can be achieved from the sizes of other peaks as well as from the intensity of the noise stripes at 0.93 ppm (P3), 1.57 ppm (P2), 2.28 ppm (T7) and 3.38 ppm (M1).

The comparison of data obtained with sequence **D**, especially with sequence **C** with similar time constants, suggests that sequence **D** with bipolar gradients results in slightly lower intensi-

ties in general, but the difference is not significant. This could arise from the two additional ^{1}H 180° pulses in sequence **C**. The separation in diffusion dimension was equal for all the iDOSY-HMBC sequences. From the sensitivity point of view, the simplest iDOSY-HMBC pulse sequence **A** performed the best. It should be remembered, however, that for different mixture compositions with different molecular size distribution, the other variants capable of prolonging the diffusion time might prove valuable.

3. Conclusions

The iDOSY-HMBC pulse sequences presented in Fig. 1 enable recording of 3D diffusion resolved HMBC data. The extra separation obtained via the diffusion dimension can significantly simplify the HMBC data of mixtures containing analytes of different molecular sizes. In addition, the same 3D pulse sequences can be readily used in 2D-mode for diffusion filtering/editing to attenuate or even suppress the signals of fast diffusing species, for example signals from multisolvent systems, and thus simplify the 2D HMBC spectrum of the analyte of interest. For mixtures containing components of clearly different molecular sizes, ranging from small to medium-sized, or even large molecules in non-viscous solvents, the simplest pulse sequence **A** is recommended to start with, since the diffusion time within the polarization transfer delay is in most cases sufficient for proper diffusional attenuation. Obviously, a proper attenuation of the signals is required for diffusion editing (2D) and also for DOSY calculation. In case of viscous solvents, the attenuation/-suppression of small molecules might not be sufficient with the diffusion time available within the HMBC polarization transfer delay. For those cases, the pulse sequences allowing longer diffusion times can be used. The pulse sequences **B** and **D** increase the available diffusion time mildly via the duration of 3rd order low-pass filter. In addition, the pulse sequence **D** also allows free selection of diffusion gradient duration, naturally within hardware limitations, improving the efficiency of the diffusion gradient. On the other hand, if truly longer diffusion times are required, pulse sequence **C** might be useful. It should be noted, however, that for systems with very low diffusion coefficients and short T_2-values, one should select BPPSTE-based methods, as extensive diffusion times are typically needed in these cases. Generally, the presented
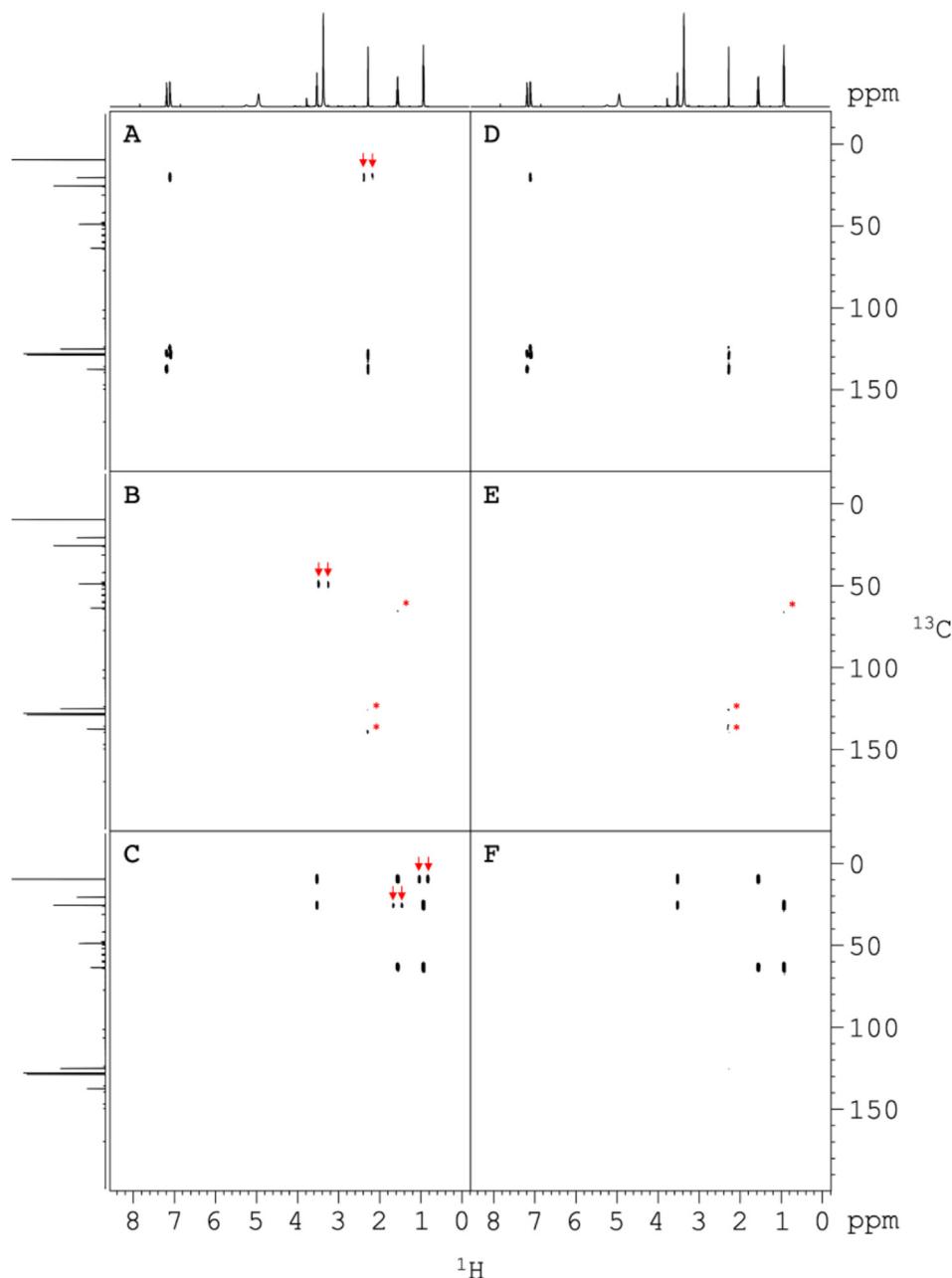
Fig. 3. 2D HMBC slices for toluene, −8.77 log(m^2/s), methanol, −8.84 log(m^2/s) and *n*-propanol, −8.92 log(m^2/s) extracted from 3D iDOSY-HMBC spectra recorded with pulse sequences **A** and **B**. The slice locations as shown in Fig. 2. Slices A-C represent HMBC spectra of toluene, methanol and n-propanol from 3D iDOSY-HMBC data recorded using pulse sequence **A** whereas D-F are corresponding slices from data with pulse sequence **B**. Same pairwise scaling for test mixture components have been utilized (AD, BE, CF). Red arrows indicate the residual direct ^{1}H–^{13}C correlations due to imperfect low-pass filtering. These are prominent in slices A-C recorded with sequence **A** utilizing 1st order low-pass filter, whereas 3rd order filter was utilized for data shown in slices D-F. The spurious signals leaking in from other mixture component are annotated by red asterisks. Normal 1D ^{1}H- and ^{13}C-{^{1}H}-spectra are displayed on f$_2$- and f$_1$-axes. (For interpretation of the references to colour in this figure legend, the reader is referred to the web version of this article.)

methods constitute valuable tools for organic chemistry-oriented NMR, for the qualitative analysis of mixtures, as well as for simplifying 2D HMBC spectra of larger molecules via suppressing the irrelevant small molecule impurity signals or signals of complex, non-deuterated solvents.

4. Experimental

Test sample was prepared in 5 mm o.d. NMR tube by dissolving 42 mg of brucine in 0.7 ml 1:1:1:1 mixture of methanol d_4: methanol : *n*-propanol: toluene.

All NMR-experiments were performed at 25 °C using Bruker Avance NEO spectrometer (600 MHz ^{1}H-frequency) equipped with 5 mm triple resonance (^{1}H/^{19}F, ^{13}C, ^{31}P) inverse-detection probe-head equipped with triple axis gradient coils capable of delivering X-, Y- and Z-gradient amplitudes up to 50 G/cm, 50 G/cm and 67 G/cm, respectively. All the data were processed with Bruker TopSpin 4.0.4-software.

One-dimensional ^{1}H-spectrum of was recorded using 30° flip angle, spectral width of 5263 Hz covered by 32768 complex data points (6.23 s acquisition time), relaxation delay of 2.0 s, 4 steady-state scans and 64 transients. The FID was weighted by
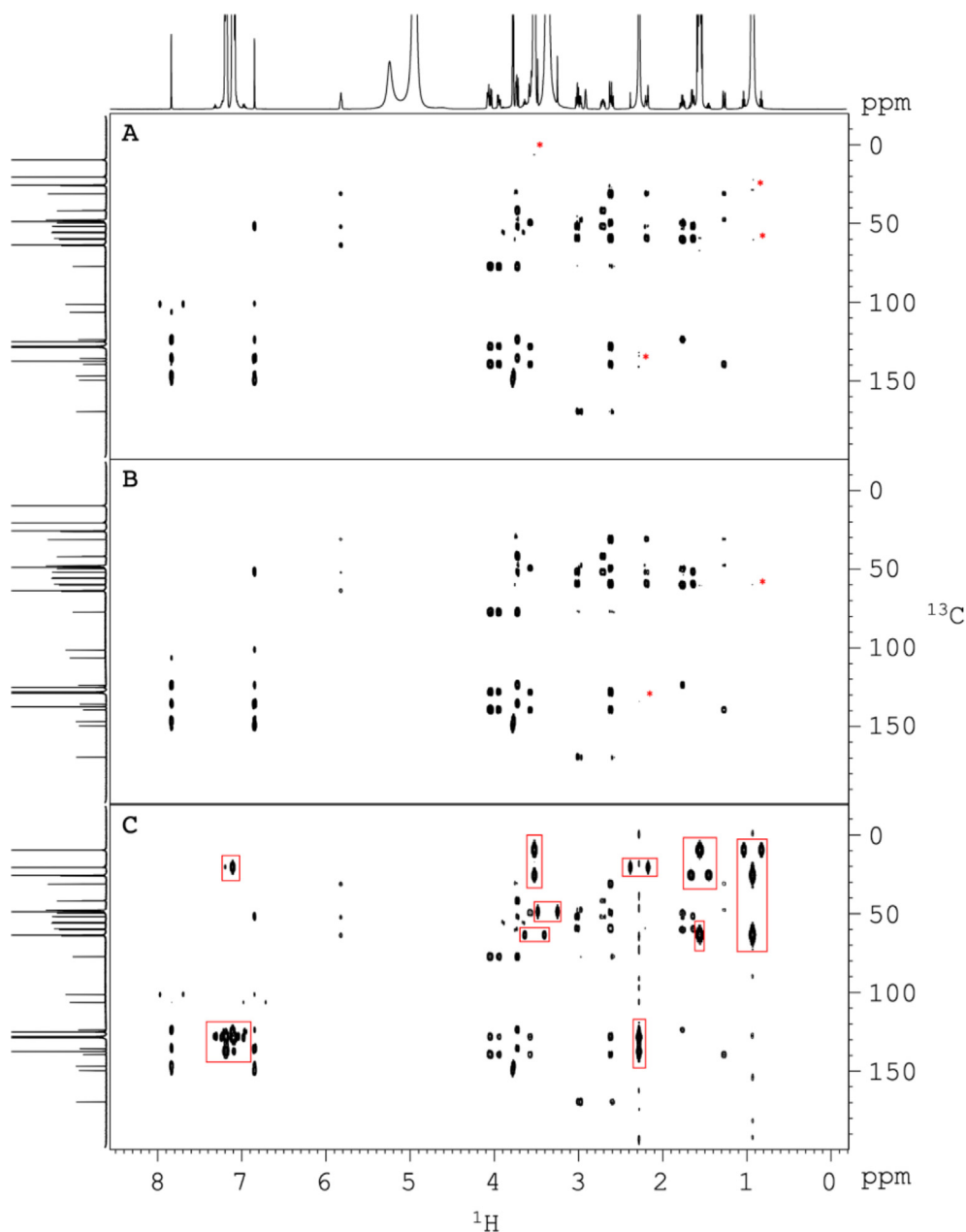
Fig. 4. 2D HMBC slices for brucine, −9.27 log(m²/s), extracted from 3D iDOSY-HMBC spectra A) recorded with pulse sequence **A** and B) recorded with pulse sequences **B** as well as C) normal gradient selected 2D HMBC measured from the same test mixture. The HMBC slices extracted from iDOSY-HMBC data are plotted using the same scaling. The signals marked by red rectangles in C) normal 2D HMBC spectrum indicate the correlation peaks of toluene, methanol and *n*-propanol. The red asterisks marked in A) and B) indicate minor spurious signals originating from high concentration, small molecule components *n*-propanol (3.34 M) and toluene (2.35 M) leaking into HMBC slice of brucine (0.15 M). The 1D ¹H- and ¹³C-{¹H}-spectra along f₂- and f₁-axes are vertically scaled up to emphasize brucine signals. (For interpretation of the references to colour in this figure legend, the reader is referred to the web version of this article.)

exponential function with 0.3 Hz line broadening factor and zero-filled up to 65,536 complex points prior to Fourier transformation. One-dimensional ¹H-spectrum of was recorded using 30° flip angle, spectral width of 5263 Hz covered by 32768 complex data points (6.23 s acquisition time), relaxation delay of 2.0 s, 4 steady-state scans and 64 transients. The FID was weighted by exponential function with 0.3 Hz line broadening factor and zero-filled up to 65536 complex points prior to Fourier transformation.

One-dimensional ¹³C-{¹H}-spectrum of was recorded using 30° flip angle, WALTZ-65 ¹H-decoupling scheme,[55] spectral width of 32680 Hz covered by 32768 complex data points (1.00 s acquisition time), relaxation delay of 2.0 s, 16 steady-state scans and

4096 transients. The FID was weighted by exponential function with 1.0 Hz line broadening factor prior to Fourier transformation.

For 3D iDOSY-HMBC experiments (pulse sequences **A**-**D**) the spectral widths (carrier positions) were 5263 Hz (4.18 ppm) and 33174 Hz (90.00 ppm) in ¹H- and ¹³C-dimensions, respectively. The experiments were acquired using 64 steady-state scans, 4 transients and data matrix size of 1024 (¹H, complex points) × 20 (diffusion gradient steps) × 64 (¹³C, complex points). The FID-acquisition time was 194.56 ms and the duration of the last t₁-increment (t₁max) was 1.93 ms. The diffusion steps were accomplished by recording 20 HMBC datasets with linearly increasing diffusion gradient (Z) strength from 3.0 G/cm to 48.2 G/cm. The
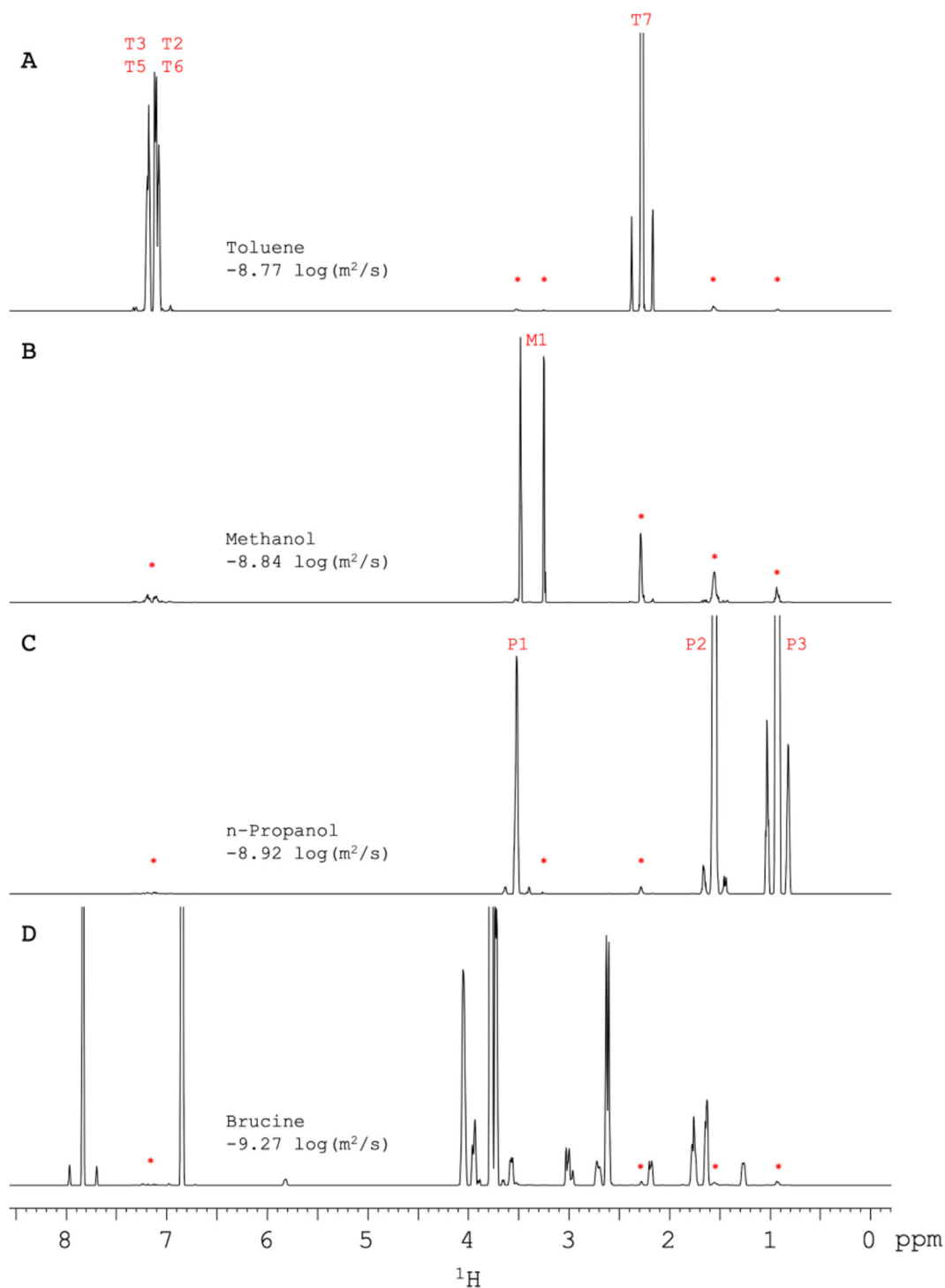
Fig. 5. 1D ^{1}H-projections extracted from HMBC slices (Fig. 3A-3C, 4A) of individual test mixture components, A) toluene, B) methanol, C) *n*-propanol and D) brucine. The logD-value of the corresponding HMBC slice is also shown. The red asterisks in the projections indicate spurious signals originating from other mixture components. The assignments for faster diffusing components methanol, *n*-propanol and toluene are included. (For interpretation of the references to colour in this figure legend, the reader is referred to the web version of this article.)

data was zero filled up to 2048 complex points in ^{1}H-dimension and forward-linear-predicted up to 512 complex points in ^{13}C-dimension. Sine squared apodization was applied to both dimensions prior to Fourier transformation. Magnitude mode 2D spectra were calculated. Pulses: ^{1}H 90° = 10.9 μs; ^{13}C 90° = 17.0 μs; frequency swept adiabatic wideband ^{13}C-pulse AS = 500 μs (smoothed CHIRP [51], bandwidth 60 kHz, RF-power 9.8 kHz). Delays: relaxation delay = 2.0 s, τ_e (eddy current recovery delay)

= 200 μs, Δ_D = 67.5 ms (sequence **A**), 81.5 ms (sequence **B**), 80.0 ms (sequence **C**) and 83.2 ms (sequence **D**) and Δ_{LR} = 71.4 ms (optimized for $^nJ_{CH}$ of 7.0 Hz). Delay δ_1 for sequence **B** was 5.99 ms corresponding to Δ_D of 80 ms. The delay δ_2 for sequence **D** was 239 μs. The low-pass filter delays were calculated using values 145 Hz, 120 Hz and 170 Hz for $^1J_{CHave}$, $^1J_{CHmin}$ and $^1J_{CHmax}$, respectively, resulting in τ = 3.45 ms, τ_1 = 4.05 ms, τ_2 = 3.45 ms, τ_3 = 3.00 ms. Diffusion gradient (g_D) duration δ_D was 2.5 ms. Other
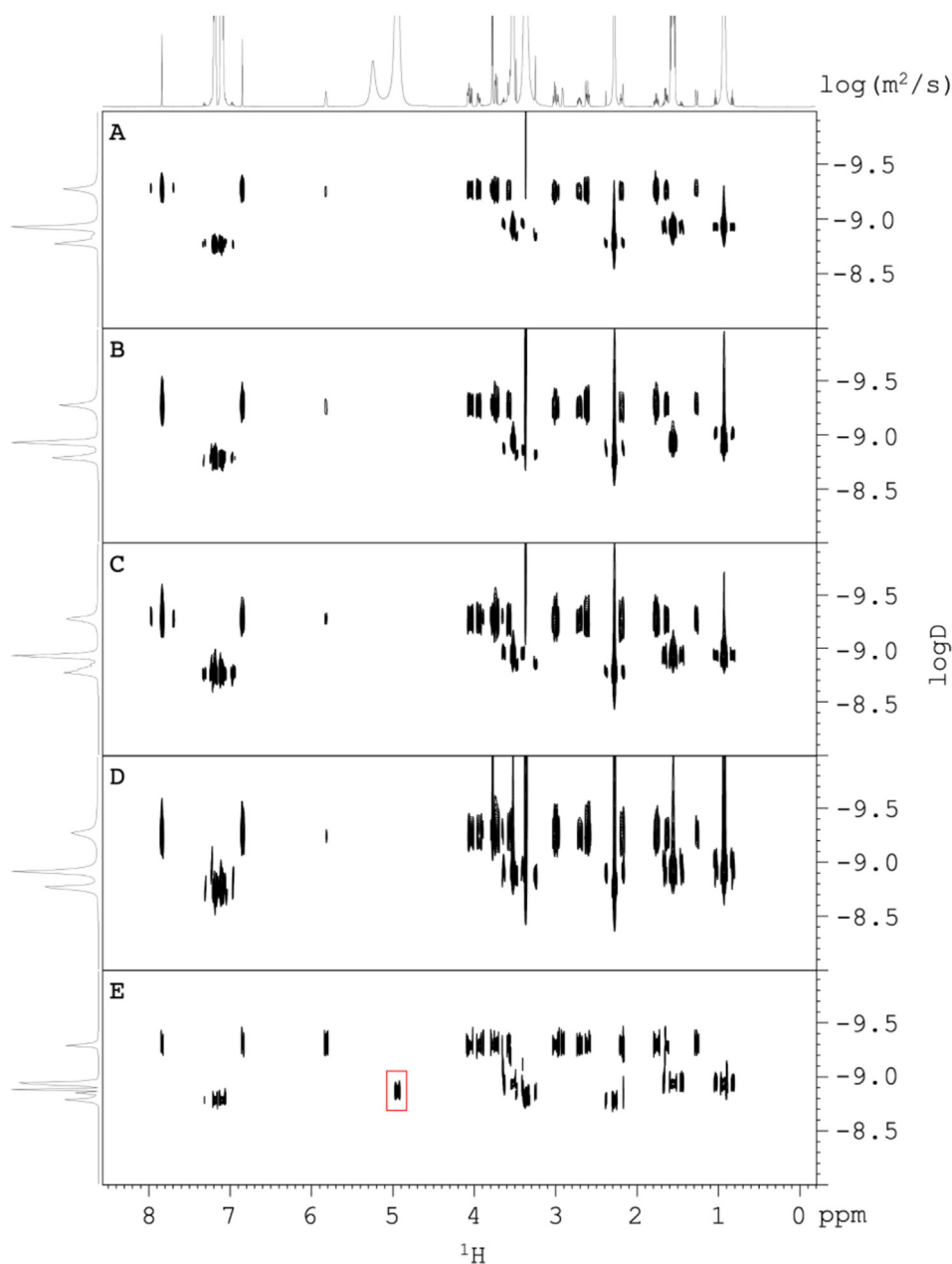
Fig. 6. 2D ^{1}H DOSY projections of 3D iDOSY-HMBC spectra recorded using pulse sequences shown in Fig. 1. Fig. 6A–D correspond to the pulse sequences **A-D**, respectively. In addition, a normal 2D ^{1}H DOSY recorded using BPPSTE-LED-pulse sequence [7,8] is presented in Fig. 6E for comparison. The extracted 2D projections correspond to the sum of data taken along the ^{13}C chemical shift axis. Individual vertical scaling was utilized for each 2D spectrum. 1D ^{1}H-spectrum along f_2-axis (top) is vertically scaled up to emphasize brucine signals. The diffusion projections (logD) on the left have been calculated by taking sum along the ^{1}H-axis. The DOSY correlation indicated by a red rectangle corresponds to the residual signal of water and methanol hydroxyl protons.

gradient durations: g_1-g_7 = 1.0 ms. Gradient strengths in percentages (axis): g_D = 5–80% (Z), g_1 = 14% (Y) 1st order low-pass filter, 21% (Y) 3rd order low pass filter, g_2 = -12% (Y), g_3 = -6% (Y), g_4 = -3%(Y), g_5 = 25% (XZ), g_6 = 15% (XZ), g_7 = 20.05% (XZ). Smoothed square shape was used for all the gradients (100 points, 10-point ramp up/ramp down). All 2D HMBC datapoints form an array of 20 points of attenuating intensities along the diffusional decay dimension. Diffusion coefficients and corresponding line widths (from fitting error) were individually calculated for all points exceeding the noise threshold in the first 2D HMBC plane using Levenberg-Marquardt algorithm [56,57] to fit the data with Stejskal-Tanner equation (Equation (1)) [6,11,17]. The shape factor (σ_D) was 0.9 for the utilized gradient shape. The value for delay $\varDelta'$ (Eq. (1)) was calculated as shown in Eq. (6).

$$\varDelta' = \Delta_D - \frac{\delta_D}{3} - \frac{\tau_D}{2} \tag{6}$$

The delay τ_D in Eq. (6) was set to 0 ms for gradient echo pulse sequences **A-C** and 0.7 ms for pulse sequence **D** utilizing bipolar diffusion gradient pulses. Diffusion gradient shape effects [18] on $\varDelta'$ were not applied (the difference between the gradient shape effect-corrected and uncorrected $\varDelta'$ would have been very small compared to Δ_D, 81 μs and 20 μs for pulse sequences **A-C** and **D**, respectively). The low-pass filter gradients during Δ_D in pulse sequences **B** and **D** were applied along different gradient axis (Y) to that of diffusion gradients (Z) and thus would not require alteration in $\varDelta'$. In general, the experiments presented here are not aimed for measuring quantitative diffusion coefficient data but

instead for providing extra separation in diffusion domain. Therefore, the utilization of basic form of the Stejskal-Tanner equation, is acceptable for most cases to generate the DOSY-dimension. Single exponential behavior was assumed *i.e.* one diffusion decay per HMBC datapoint was calculated. Fitting limits were 0–10^{-8} m^2/s and the 3D spectrum was created for diffusion coefficient range of 10^{-10}-10^{-8} m^2/s. Maximum number of iterations was 100, spike suppression factor 4 and DOSY line width factor 2 were used. In the final 3D spectrum, 128 points and logarithmic scale were used to present the DOSY dimension.

Normal gradient selected HMBC spectrum with 1st order low-pass filter (phase cycled) was recorded using similar measurement parameters as were used in iDOSY-HMBC experiments, except for the coherence selection gradients which were all applied along Z-axis with gradient strength percentages 50%:30%:40.1%. Reference 2D ^{1}H DOSY was recorded using BPPSTE-LED pulse sequence [7,8] with the spectral width (carrier position) of 5263 Hz (4.18 ppm), 64 steady-state scans, 32 transients and data matrix size of 8192 (^{1}H, complex points) $\times$ 20 (diffusion gradient steps). The FID-acquisition time was 1.56 s. The diffusion steps were performed by recording 20 spectra linearly increasing diffusion gradient strength from 3.0 G/cm to 48.2 G/cm. The first 2048 complex points of the data were subject to sine squared apodization and Fourier transformation. Magnitude mode calculation was performed prior to the Stejskal-Tanner equation fitting to construct the diffusion dimension (see above). DOSY processing was identical to iDOSY-HMBC experiments. Pulses: ^{1}H 90° = 11.0 μs; Delays: relaxation delay = 2.0 s, τ_e (eddy current recovery delay) = 200 μs, Δ_D = 80.0 ms, τ_D = 0.222 ms and longitudinal eddy current delay = 5.0 ms. Diffusion gradient duration δ_D was 2.5 ms (two 1.25 ms gradient pulses of opposite polarities) and strength was linearly varied from 5% to 80%. The spoiler gradient durations during the diffusion time and longitudinal eddy current delay were both 600 μs and the strengths were -17.13% and -13.17%, respectively. All the gradients were applied along Z-axis in BPPSTE-LED experiment.

Declaration of Competing Interest

The authors declare that they have no known competing financial interests or personal relationships that could have appeared to influence the work reported in this paper.

Appendix A. Supplementary material

Supplementary data to this article can be found online at https://doi.org/10.1016/j.jmr.2020.106892.

References

[1] H. Barjat, G.A. Morris, S. Smart, A.G. Swanson, S.C.R. Williams, High-resolution diffusion-ordered 2D spectroscopy (HR-DOSY) – a new tool for the analysis of complex-mixtures, J. Magn. Reson. B 108 (1995) 170–172.

[2] K.F. Morris, C.S. Johnson, Diffusion-ordered two-dimensional nuclear magnetic resonance spectroscopy, J. Am. Chem. Soc. 114 (1992) 3139–3141.

[3] K.F. Morris, C.S. Johnson, Resolution of discrete and continuous molecular size distributions by means of diffusion-ordered 2D NMR spectroscopy, J. Am. Chem. Soc. 115 (1993) 4291–4299.

[4] D.P. Hinton, C.S. Johnson, Diffusion ordered 2D NMR spectroscopy of phospholipid vesicles: determination of vesicle size distributions, J. Phys. Chem. 97 (1993) 9064–9072.

[5] S.J. Gibbs, C.S. Johnson, A PFG NMR experiment for accurate diffusion and flow studies in the presence of eddy currents, J. Magnet. Reson. 93 (1991) (1969) 395–402.

[6] C.S. Johnson, Diffusion ordered nuclear magnetic resonance spectroscopy: principles and applications, Prog. Nucl. Magn. Reson. Spectrosc. 34 (1999) 203–256.

[7] D.H. Wu, A.D. Chen, C.S. Johnson, An improved diffusion-ordered spectroscopy experiment incorporating bipolar-gradient pulses, J. Magn. Reson. A 115 (1995) 260–264.

[8] M.D. Pelta, H. Barjat, G.A. Morris, A.L. Davis, S.J. Hammond, Pulse sequences for high-resolution diffusion-ordered spectroscopy (HR-DOSY), Magn. Reson. Chem. 36 (1998) 706–714.

[9] D.H. Wu, A.D. Chen, C.S. Johnson, Three-dimensional diffusion-ordered NMR spectroscopy: The homonuclear COSY-DOSY experiment, J. Magn. Reson. A 121 (1996) 88–91.

[10] E.K. Gozansky, D.G. Gorenstein, DOSY-NOESY: diffusion-ordered NOESY, J. Magn. Reson. B 111 (1996) 94–96.

[11] A. Jerschow, N. Müller, 3D Diffusion-ordered TOCSY for slowly diffusing molecules, J. Magn. Reson. A 123 (1996) 222–225.

[12] L.H. Lucas, W.H. Otto, C.K. Larive, The 2D-J-DOSY experiment: resolving diffusion coefficients in mixtures, J. Magn. Reson. 156 (2002) 138–145.

[13] D. Wu, A. Chen, J. Johnson Charles S., Heteronuclear-detected diffusion-ordered NMR spectroscopy through coherence transfer, J. Magn. Reson. A 123 (1996) 215–218.

[14] H. Barjat, G.A. Morris, A.G. Swanson, A three-dimensional DOSY-HMQC experiment for the high-resolution analysis of complex mixtures, J. Magn. Reson. 131 (1998) 131–138.

[15] T. Brand, E.J. Cabrita, G.A. Morris, R. Günther, H.-J. Hofmann, S. Berger, Residue-specific NH exchange rates studied by NMR diffusion experiments, J. Magn. Reson. 187 (2007) 97–104.

[16] T. Didenko, R. Boelens, S.G.D. Rudiger, 3D DOSY-TROSY to determine the translational diffusion coefficient of large protein complexes, Protein Eng. Des. Sel. 24 (2011) 99–103.

[17] E.O. Stejskal, J.E. Tanner, Spin diffusion measurements: spin echoes in the presence of a time-dependent field gradient, J. Chem. Phys. 42 (1965) 288–292.

[18] D. Sinnaeve, The Stejskal-Tanner equation generalized for any gradient shape—an overview of most pulse sequences measuring free diffusion, Concepts Magn. Reson. 40A (2012) 39–65.

[19] R. Evans, I.J. Day, Matrix-assisted diffusion-ordered spectroscopy, RSC Adv. 6 (2016) 47010–47022.

[20] C. Carrara, S. Viel, C. Delaurent, F. Ziarelli, G. Excoffier, S. Caldarelli, Chromatographic NMR in NMR solvents, J. Magn. Reson. 194 (2008) 303–306.

[21] S. Viel, F. Ziarelli, S. Caldarelli, Enhanced diffusion-edited NMR spectroscopy of mixtures using chromatographic stationary phases, Proc. Natl. Acad. Sci. USA 100 (2003) 9696–9698.

[22] R.E. Hoffman, H. Arzuan, C. Pemberton, A. Aserin, N. Garti, High-resolution NMR "chromatography" using a liquids spectrometer, J. Magn. Reson. 194 (2008) 295–299.

[23] R. Evans, A. Hernandez-Cid, G. Dal Poggetto, A. Vesty, S. Haiber, G.A. Morris, M. Nilsson, Matrix-assisted diffusion-ordered NMR spectroscopy with an invisible matrix: a vanishing surfactant, RSC Adv. 7 (2017) 449–452.

[24] R.W. Adams, J.A. Aguilar, J. Cassani, G.A. Morris, M. Nilsson, Resolving natural product epimer spectra by matrix-assisted DOSY, Org. Biomol. Chem. 9 (2011) 7062–7064.

[25] I.J. Day, Matrix-assisted DOSY, Prog. Nucl. Magn. Reson. Spectrosc. 116 (2020) 1–18.

[26] K.S. Salome, C.F. Tormena, Enantiodiscrimination by matrix-assisted DOSY NMR, ChemComm. 55 (2019) 8611–8614.

[27] J.S. Kavakka, I. Kilpeläinen, S. Heikkinen, General chromatographic NMR method in liquid state for synthetic chemistry: polyvinylpyrrolidone assisted DOSY experiments, Org. Lett. 11 (2009) 1349–1352.

[28] J.S. Kavakka, V. Parviainen, K. Wähälä, I. Kilpeläinen, S. Heikkinen, Enhanced chromatographic NMR with polyethyleneglycol. A novel resolving agent for diffusion ordered spectroscopy, Magn. Reson. Chem. 48 (2010) 777–781.

[29] M. Zanatta, V.U. Antunes, C.F. Tormena, J. Dupont, F.P. dos Santos, Dealing with supramolecular structure for ionic liquids: a DOSY NMR approach, Phys. Chem. Chem. Phys. 21 (2019) 2567–2571.

[30] L. Avram, Y. Cohen, Diffusion NMR of molecular cages and capsules, Chem. Soc. Rev. 44 (2015) 586–602.

[31] F. Elwinger, J. Wernersson, I. Furó, Quantifying size exclusion by diffusion NMR: A versatile method to measure pore access and pore size, Anal. Chem. 90 (2018) 11431–11438.

[32] Peter C. M van Zijl, C.T.W. Moonen, Complete water suppression for solutions of large molecules based on diffusional differences between solute and solvent (DRYCLEAN), J. Magn. Reson. 87 (1990) 18–25.

[33] A.W.T. King, V. Mäkelä, S.A. Kedzior, T. Laaksonen, G.J. Partl, S. Heikkinen, H. Koskela, H.A. Heikkinen, A.J. Holding, E.D. Cranston, I. Kilpeläinen, Liquid-State NMR analysis of nanocelluloses, Biomacromolecules 19 (2018) 2708–2720.

[34] D.R. del Cerro, T.V. Koso, T. Kakko, A.W.T. King, I. Kilpeläinen, Crystallinity reduction and enhancement in the chemical reactivity of cellulose by non-dissolving pre-treatment with tetrabutylphosphonium acetate, Cellulose 27 (2020) 5545–5562.

[35] N. Birlirakis, E. Guittet, A new approach in the use of gradients for size-resolved 2D-NMR experiments, J. Am. Chem. Soc. 118 (1996) 13083–13084.

[36] B. Vitorge, D. Jeannerat, NMR diffusion measurements in complex mixtures using constant-time-HSQC-IDOSY and computer-optimized spectral aliasing for high resolution in the carbon dimension, Anal. Chem. 78 (2006) 5601–5606.

[37] A.S. McLachlan, J.J. Richards, A.R. Bilia, G.A. Morris, Constant time gradient HSQC–iDOSY: practical aspects, Magn. Reson. Chem. 47 (2009) 1081–1085.

[38] M.J. Stchedroff, A.M. Kenwright, G.A. Morris, M. Nilsson, R.K. Harris, 2D and 3D DOSY methods for studying mixtures of oligomeric dimethylsiloxanes, Phys. Chem. Chem. Phys. 6 (2004) 3221–3227.

[39] M. Nilsson, A.M. Gil, I. Delgadillo, G.A. Morris, Improving pulse sequences for 3D diffusion-ordered NMR spectroscopy: 2DJ-IDOSY, Anal. Chem. 76 (2004) 5418–5422.

[40] M. Nilsson, A.M. Gil, I. Delagadillo, G.A. Morris, Improving pulse sequences for 3D DOSY: COSY-IDOSY, ChemComm. (2005) 1737–1739.

[41] J.E. Power, M. Foroozandeh, P. Moutzouri, R.W. Adams, M. Nilsson, S.R. Coombes, A.R. Phillips, G.A. Morris, Very broadband diffusion-ordered NMR spectroscopy: ^{19}F DOSY, ChemComm. 52 (2016) 6892–6894.

[42] M. Foroozandeh, L. Castañar, L.G. Martins, D. Sinnaeve, G.D. Poggetto, C.F. Tormena, R.W. Adams, G.A. Morris, M. Nilsson, Ultrahigh-resolution diffusion-ordered spectroscopy, Angew. Chem. Int. Ed. 55 (2016) 15579–15582.

[43] G. Dal Poggetto, L. Castañar, R.W. Adams, G.A. Morris, M. Nilsson, Dissect and divide: Putting NMR spectra of mixtures under the knife, J. Am. Chem. Soc. 141 (2019) 5766–5771.

[44] A. Bax, M.F. Summers, Proton and carbon-13 assignments from sensitivity-enhanced detection of heteronuclear multiple-bond connectivity by 2D multiple quantum NMR, J. Am. Chem. Soc. 108 (1986) 2093–2094.

[45] R.E. Hurd, B.K. John, Gradient-enhanced proton-detected heteronuclear multiple-quantum coherence spectroscopy, J. Magn. Reson. 91 (1991) 648–653.

[46] W. Willker, D. Leibfritz, R. Kerssebaum, W. Bermel, Gradient selection in inverse heteronuclear correlation spectroscopy, Magn. Reson. Chem. 31 (1993) 287–292.

[47] J. Furrer, A comprehensive discussion of hmbc pulse sequences, part 1: The classical HMBC, Concepts Magn. Reson. 40A (2012) 101–127.

[48] M. Oouchi, J. Ukawa, Y. Ishii, H. Maeda, Structural analysis of the terminal groups in commercial hevea natural rubber by 2D-NMR with DOSY filters and multiple-WET methods using ultrahigh-field NMR, Biomacromolecules 20 (2019) 1394–1400.

[49] H. Kogler, O.W. Sørensen, G. Bodenhausen, R.R. Ernst, Low-pass J filters. Suppression of neighbor peaks in heteronuclear relayed correlation spectra, J. Magn. Reson. 55 (1983) 157–163.

[50] A. Meissner, O.W. Sørensen, Measurement of J(H, H) and long-range J(X, H) coupling constants in small molecules. Broadband XLOC and J-HMBC, Magn. Reson. Chem. 39 (2001) 49–52.

[51] J.M. Bohlen, G. Bodenhausen, Experimental aspects of chirp NMR spectroscopy, J. Magn. Reson. A 102 (1993) 293–301.

[52] D. Marion, M. Ikura, R. Tschudin, A. Bax, Rapid recording of 2D NMR-spectra without phase cycling - application to the study of hydrogen-exchange in proteins, J. Magn. Reson. 85 (1989) 393–399.

[53] A. Jerschow, N. Müller, Suppression of convection artifacts in stimulated-echo diffusion experiments. Double-stimulated-echo experiments, J. Magn. Reson 125 (1997) 372–375.

[54] M. Nilsson, G.A. Morris, Improving pulse sequences for 3D DOSY: Convection compensation, J. Magn. Reson. 177 (2005) 203–211.

[55] Z. Zhou, R. Kümmerle, X. Qiu, D. Redwine, R. Cong, A. Taha, D. Baugh, B. Winniford, A new decoupling method for accurate quantification of polyethylene copolymer composition and triad sequence distribution with ^{13}C NMR, J. Magn. Reson. 187 (2007) 225–233.

[56] W.H. Press, S.A. Teukolsky, B.P. Vetterling, B.P. Flannery, Numerical recipes in Fortran, Cambridge University Press, New York, 1992.

[57] P.R. Bevington, Data reduction and error analysis for the physical sciences, McGraw-Hill, New York, 1969.